

## Influence of Filler Pore Structure and Polymer on the Performance of MOF-Based Mixed-Matrix Membranes for CO<sub>2</sub> Capture

Sabetghadam, Anahid; Liu, Xinlei; Benzaqui, Marvin; Gkaniatsou, Effrosyni; Orsi, Angelica; Lozinska, Magdalena M.; Sicard, Clemence; Johnson, Timothy; Steunou, Nathalie; Wright, Paul A.

**DOI**

[10.1002/chem.201800253](https://doi.org/10.1002/chem.201800253)

**Publication date**

2018

**Document Version**

Accepted author manuscript

**Published in**

Chemistry - A European Journal

**Citation (APA)**

Sabetghadam, A., Liu, X., Benzaqui, M., Gkaniatsou, E., Orsi, A., Lozinska, M. M., Sicard, C., Johnson, T., Steunou, N., Wright, P. A., Serre, C., Gascon, J., & Kapteijn, F. (2018). Influence of Filler Pore Structure and Polymer on the Performance of MOF-Based Mixed-Matrix Membranes for CO<sub>2</sub> Capture. *Chemistry - A European Journal*, 24, 7949-7956. <https://doi.org/10.1002/chem.201800253>

**Important note**

To cite this publication, please use the final published version (if applicable).  
Please check the document version above.

**Copyright**

Other than for strictly personal use, it is not permitted to download, forward or distribute the text or part of it, without the consent of the author(s) and/or copyright holder(s), unless the work is under an open content license such as Creative Commons.

**Takedown policy**

Please contact us and provide details if you believe this document breaches copyrights.  
We will remove access to the work immediately and investigate your claim.

# Influence of Filler Pore Structure and Polymer on the Performance of MOF-based Mixed Matrix Membranes for CO<sub>2</sub> Capture

Anahid Sabetghadam,<sup>[a]</sup> Xinlei Liu,<sup>\*[a]</sup> Marvin Benzaqui,<sup>[b,c]</sup> Effrosyni Gkaniatsou,<sup>[b]</sup> Angelica Orsi,<sup>[e]</sup> Magdalena M. Lozinska,<sup>[e]</sup> Clemence Sicard,<sup>[b]</sup> Timothy Johnson,<sup>[d]</sup> Nathalie Steunou,<sup>[b]</sup> Paul A. Wright,<sup>[e]</sup> Christian Serre,<sup>[c]</sup> Jorge Gascon,<sup>[a,f]</sup> and Freek Kapteijn<sup>\*[a]</sup>

**Abstract:** In order to gain insight into the influence of metal-organic framework (MOF) filler and polymer on membrane performance, eight different composites are studied by combining four MOFs and two polymers. MOF materials (NH<sub>2</sub>-MIL-53(Al), MIL-69(Al), MIL-96(Al) and ZIF-94) with various chemical functionalities, topologies, and dimensionalities of porosity were employed as fillers, while two typical polymers with different permeability-selectivity properties (6FDA-DAM and Pebax) were deliberately selected as matrices. The best performing MOF-polymer composites were prepared by loading 25 wt.% of MIL-96(Al) as filler which improved the permeability and selectivity of 6FDA-DAM up to 32% and 10%, while for Pebax this enhancement was 25% and 18%, respectively. The observed differences in membrane performance in the separation of CO<sub>2</sub> from N<sub>2</sub> are explained on the basis of gas solubility, diffusivity properties and compatibility between the filler and polymer phases.

## Introduction

In recent times, the sharply rising atmospheric CO<sub>2</sub> concentration has generated widespread environmental

concerns.<sup>[1-3]</sup> It is clear that the earth temperature has a direct dependence on the CO<sub>2</sub> concentration, and the climate will be significantly affected with a rise of a few degrees Celsius.<sup>[1]</sup> The excessive CO<sub>2</sub> emission stems predominantly from the increasing combustion of fossil fuels due to growing industrialisation.<sup>[1-3]</sup> Currently, the most frequent method for CO<sub>2</sub> capture from a post-combustion flue gas is chemical absorption. However, this process consumes considerable energy and poses additional environmental concerns.<sup>[4]</sup>

In contrast, membrane gas separation units are gaining increasing attention not only in terms of a relatively low energy consumption and ease of operation,<sup>[5, 6]</sup> but also because of environmental aspects. To date, polymeric membranes dominate the membrane market for industrial gas separation due to their easy processing and mechanical strength.<sup>[7]</sup> Nevertheless, the limited chemical and thermal stability of existing polymeric membrane materials limits their application range. Another drawback of polymeric membranes is the known Robeson upper bound limit.<sup>[8-10]</sup> Improvement in selectivity is always sacrificing permeability, and *vice versa*. Compared with polymeric materials, inorganic membrane materials (e.g., carbon,<sup>[11]</sup> zeolites<sup>[12, 13]</sup> and metal-organic frameworks<sup>[12, 13]</sup>) always provide superior performance and stability for gas separation. However, more research effort has to be devoted to inorganic membranes to overcome their inherent obstacles, such as high cost, brittleness and lack of reproducibility.

Mixed matrix membranes (MMMs), consisting of composites of inorganic or organic fillers dispersed in a polymer phase, are proposed as alternative materials delivering both the promising performance benefits from embedded fillers and the economical processing features of polymers.<sup>[4, 14, 15]</sup> Metal-organic frameworks (MOFs) have emerged as a family of outstanding porous crystalline materials.<sup>[16-19]</sup> Their rich chemistry and topological variety render MOFs as superior fillers to construct MMMs.<sup>[20-42]</sup> However, in spite of a clear explosion in the number of publications dealing with MOF based mixed matrix membranes, clear structural property relationships for these composites and the influence of MOF structure on pore dimensionality and accessibility have not yet been established.<sup>[41, 42]</sup> More comparative studies using diverse MOF fillers and polymers are required to determine the optimal combinations and ruling variables to facilitate the development of such structure/performance correlations.

[a] A. Sabetghadam, Dr. X. Liu, Prof. Dr. J. Gascon, Prof. Dr. F. Kapteijn  
Catalysis Engineering - ChemE, Delft University of Technology, Van der Maasweg 9, 2629HZ Delft, The Netherlands  
Email: x.liu-8@tudelft.nl; f.kapteijn@tudelft.nl

[b] Dr. M. Benzaqui, E. Gkaniatsou, Dr. C. Sicard, Prof. N. Steunou  
Institut Lavoisier de Versailles, UMR CNRS 8180, Université de Versailles St Quentin en Yvelines, Université Paris Saclay, 45 av. des Etats-Unis 78035 Versailles, France

[c] Dr. M. Benzaqui, Dr. C. Serre  
Institut des Matériaux Poreux de Paris, FRE 2000 CNRS, Ecole Normale Supérieure, Ecole Supérieure de Physique et des Chimie Industrielles de Paris, PSL Research University, 75005 Paris, France

[d] Dr. T. Johnson  
Johnson Matthey Technology Centre, Blount's Court Road, Sonning Common, Reading, RG4 9NH, United Kingdom

[e] A. Orsi, Dr. M. M. Lozinska, Prof. Dr. P. A. Wright  
EaStCHEM School of Chemistry, University of St Andrews, Purdie Building, North Haugh, St Andrews, Fife, KY16 9ST, United Kingdom

[f] Prof. Dr. J. Gascon  
King Abdullah University of Science and Technology, KAUST Catalysis Center, Advanced Catalytic Materials, Thuwal 23955, Saudi Arabia

Supporting information for this article is given via a link at the end of the document.

In this study, four types of MOF materials (NH<sub>2</sub>-MIL-53(Al), MIL-69(Al), MIL-96(Al) and ZIF-94) with different chemical functionalities and topologies were studied as fillers. Two typical polymers (polyimide 6FDA-DAM and poly(ether-block-amide) Pebax) were deliberately selected as matrices because of their outstanding separation performance. The morphology, CO<sub>2</sub> adsorption properties, crystalline structures of the MOF fillers and MOF-MMMs were characterized, followed by gas permeation studies. The resulting membranes exhibit different performances in the separation of CO<sub>2</sub> / N<sub>2</sub> that can be rationalized on the basis of gas solubility and diffusivity in the MOF-MMMs, the interaction between both components of the composite and pore dimensionality.

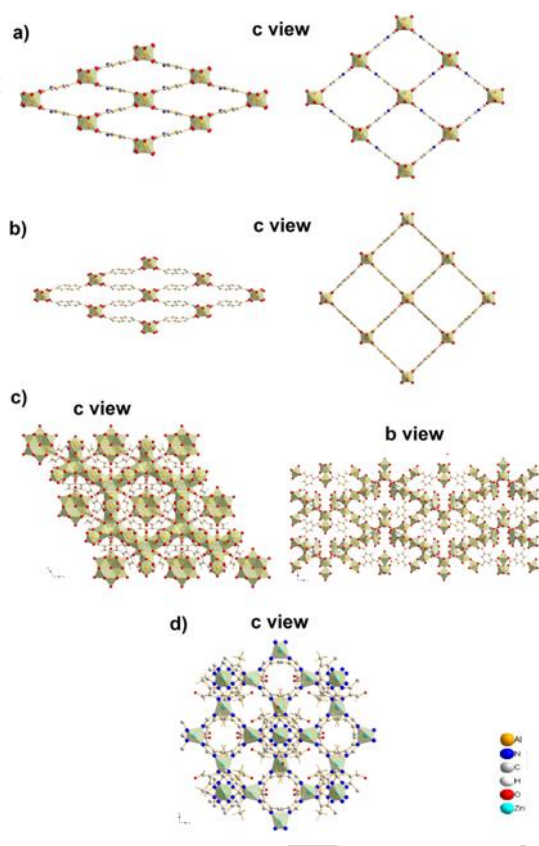


**Figure 1.** Crystalline structures of NH<sub>2</sub>-MIL-53(Al) (a, narrow and large pore forms), MIL-69(Al)/DUT-4 (b, narrow and open pore forms), MIL-96(Al) (c) and ZIF-94 (d).

NH<sub>2</sub>-MIL-53(Al),<sup>[43]</sup> with a formula Al(OH)[O<sub>2</sub>C–C<sub>6</sub>H<sub>3</sub>NH<sub>2</sub>–CO<sub>2</sub>], is isoreticular to the well-known MIL-53.<sup>[44]</sup> This material is a microporous framework with diamond-shaped 1D channels (Figure 1a), which presents excellent properties for the selective adsorption of CO<sub>2</sub>.<sup>[45]</sup> In this framework, dispersion forces control the flexibility of the structure: its narrow pore (*np*, window size ~3.4×16.0 Å<sup>2</sup>)

form is preferred at low CO<sub>2</sub> pressures, while the framework expands to its large pore (*lp*, window size ~8.5×12.0 Å<sup>2</sup>) form at high CO<sub>2</sub> partial pressures.<sup>[46]</sup> NH<sub>2</sub>-MIL-53 has been reported to display outstanding selectivity in the separation of CO<sub>2</sub> from natural gas or flue gas.<sup>[4,35]</sup> For comparative studies, another MOF material with similar topology was selected, i.e. MIL-69(Al) (formulated Al(OH)[O<sub>2</sub>C–C<sub>10</sub>H<sub>6</sub>–CO<sub>2</sub>]).<sup>[47]</sup> This also is a microporous network with diamond-shaped 1D tunnels and a window size around 2.7×13.6 Å<sup>2</sup> in its narrow pore form upon hydrothermal synthesis, and 8.5×8.5 Å<sup>2</sup> in its anhydrous form (open square-like pore) which is called DUT-4 (Figure 1b).<sup>[48]</sup> In contrast to the breathing phenomenon encountered in the MIL-53 series, MIL-69(Al) displays a very limited flexibility upon adsorbate uptake and removal.<sup>[48]</sup> Apart from MOFs with 1D channels, MIL-96(Al) (Al<sub>12</sub>O(OH)<sub>16</sub>(H<sub>2</sub>O)<sub>5</sub>[btc]<sub>6</sub>•29H<sub>2</sub>O, btc = 1,3,5-benzene-tricarboxylate)<sup>[49]</sup> is a trimesate microporous MOF which its structure has recently been refined and exhibits a 2D pore network. The MOF structure has three types of cavities. Of these cavities, only the B- and C-types are accessible, creating a “zigzag” 2D pore network with shared windows (4.5×3.6 Å<sup>2</sup>) (Figure 1c).<sup>[49]</sup> After thermal activation, some water molecules, located on the μ<sub>3</sub>-oxo Al trimer, are removed, which may increase the window diameter by approximately 2 Å.<sup>[51]</sup> MIL-96/Matrimid MMMs were developed showing higher H<sub>2</sub> and CO<sub>2</sub> permeabilities with slightly reduced H<sub>2</sub>/CO<sub>2</sub> selectivities in comparison with the neat Matrimid membranes.<sup>[26]</sup> ZIF-94<sup>[52]</sup> (also termed as SIM-1<sup>[53]</sup> and ZIF-8-MCIM<sup>[54]</sup>), with a formula Zn[mcim]<sub>2</sub> (mcim = 4-methylimidazolate-5-carbaldehyde), is an analogue of the extensively-studied ZIF-8.<sup>[55]</sup> It has a SOD topology with a 3D pore network and a window diameter of circa 2.6 Å (Figure 1d). ZIF-94 was selected against other ZIF materials due to its high CO<sub>2</sub> uptake at low pressure.<sup>[52]</sup> As it was reported by Aguado et al.<sup>[56]</sup> and Cacho-Bailo et al.,<sup>[57]</sup> the pure ZIF-94 polycrystalline membranes exhibited good CO<sub>2</sub> selectivity (4.5 and 38) over N<sub>2</sub> and CH<sub>4</sub>, respectively.

Polyimide 6FDA-DAM is a representative glassy polymer (Figure 2a). 6FDA-DAM based membranes usually deliver a high CO<sub>2</sub> permeability and moderate CO<sub>2</sub> / N<sub>2</sub> selectivity.<sup>[4]</sup> Pebax 1657 is a benchmark block copolymer, consisting of polyether blocks (flexible segments) and polyamide backbones (rigid segments) (Figure 2b). This polymer displays higher CO<sub>2</sub> / N<sub>2</sub> selectivity and a lower CO<sub>2</sub> permeability than 6FDA-DAM.<sup>[4]</sup>

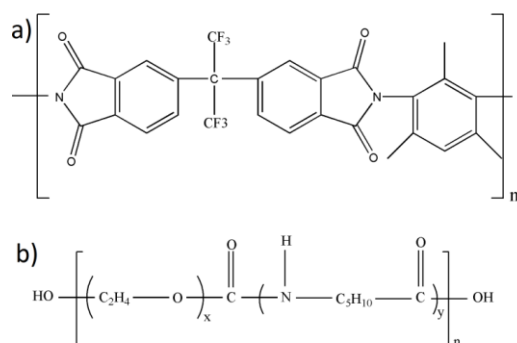


**Figure 2.** Chemical structures of polymers 6FDA-DAM (a) and Pebax 1657 (b).

## Results and Discussion

### MOF characterization

To get comparable results, the size of all synthesized MOF particles is in the sub-micrometer range (Figure 3). NH<sub>2</sub>-MIL-53(Al) displays diamond- and rod-shapes with average particle size of 500 ± 90 nm. MIL-69(Al) adopts the shape of platelets (450 ± 90 nm), while MIL-96(Al) and ZIF-94 particles are of spherical shape (150 ± 90 and 300 ± 90 nm, in size, respectively). XRD patterns demonstrate the absence of additional phases for all four samples (Figure S1).

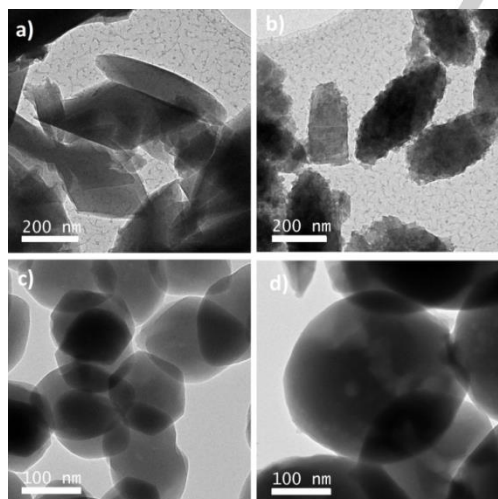


**Figure 3.** TEM images of a) NH<sub>2</sub>-MIL-53(Al), b) MIL-69(Al), c) MIL-96(Al) and d) ZIF-94.

The surface area and porosity of the MOF materials were assessed by measuring the N<sub>2</sub> adsorption isotherms at 77 K (Figure 4). The adsorption isotherms for the MOFs can be categorized as Type I, which confirms their permanent micro-porosity. The BET analysis depicts that MIL-96(Al)

has the highest surface area (Table 1), followed by ZIF-94 and MIL-69(Al). The BET areas of MIL-96(Al) and ZIF-94 are in line with previous studies.<sup>[51, 52]</sup> As previously reported, NH<sub>2</sub>-MIL-53(Al) displays hardly any uptake of N<sub>2</sub> at 77 K in its *np* configuration.<sup>[59]</sup> The pores of NH<sub>2</sub>-MIL-53(Al) start to open when *P* reaches a value of approximately 0.3 bar. Moreover, the N<sub>2</sub> desorption branch does not return at all to the adsorption branch, indicative for diffusion limitations of the N<sub>2</sub>. Therefore, no BET area is given for this MOF.

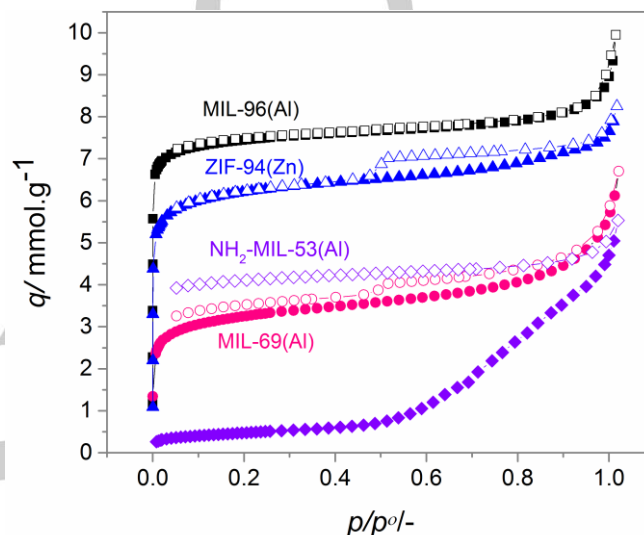


**Figure 4.** N<sub>2</sub> (77 K) adsorption (solid symbols) and desorption isotherms (open symbols) for the MOF materials.

**Table 1** BET area, pore volume, CO<sub>2</sub> uptake (@ 295 K, 1.0 bar), shape and size of the MOFs used.

MOF	$S_{BET}$ (m <sup>2</sup> /g)	$V_{micro}$ (cm <sup>3</sup> /g)	CO <sub>2</sub> uptake (mmol / g)	Shape	Particle size (nm)
NH <sub>2</sub> -MIL-53(Al)	-	-	1.6	Diamond-rod	500 ± 90
MIL-69(Al)	275	0.09	1.5	Platelet	450 ± 90
MIL-96(Al)	670	0.24	3.5	Sphere	150 ± 90
ZIF-94	545	0.20	2.3	Sphere	300 ± 90

Adsorption properties are usually critical in determining membrane performance. For this reason, we measured CO<sub>2</sub> adsorption isotherms on all MOF samples, which display a large CO<sub>2</sub> capacity at moderate pressures (Figure S3 and Table 1).



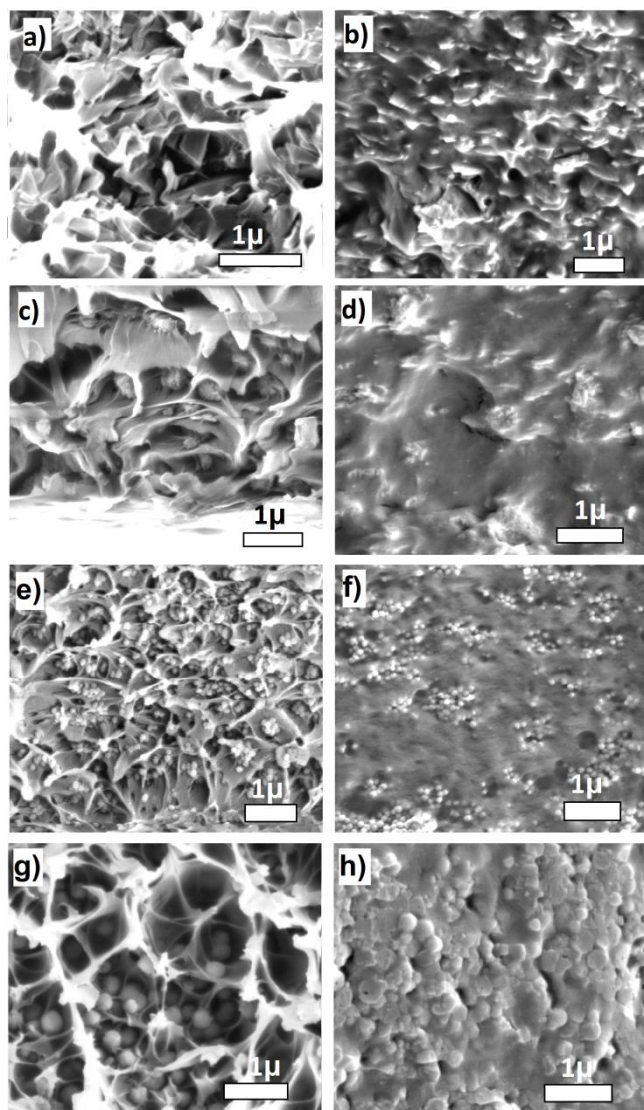


**Figure 5.** Cross sectional SEM images of MOF-6FDA-DAM (left column) and MOF-Pebax membranes (right column), both with 25 wt. % filler loadings. The embedded MOF particles in these MMMs are  $\text{NH}_2\text{-MIL-53(Al)}$  (a, b),  $\text{MIL-69(Al)}$  (c, d),  $\text{MIL-96(Al)}$  (e, f) and  $\text{ZIF-94}$  (g, h). The membrane specimens were prepared by cryo-fracturing after immersion in liquid  $\text{N}_2$  and coated with gold.

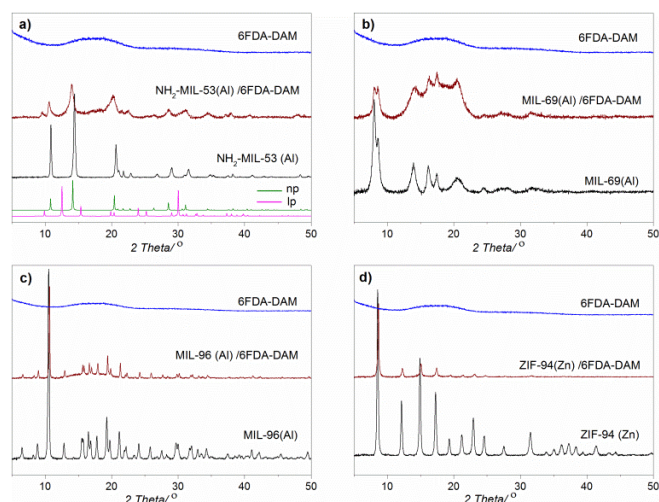


**Figure 6.** The XRD patterns of the MOF fillers, neat 6FDA-DAM membranes and MMMs. The simulated XRD patterns of  $\text{NH}_2\text{-MIL-53(Al)}$  (*lp* and *np* forms) are shown for reference.

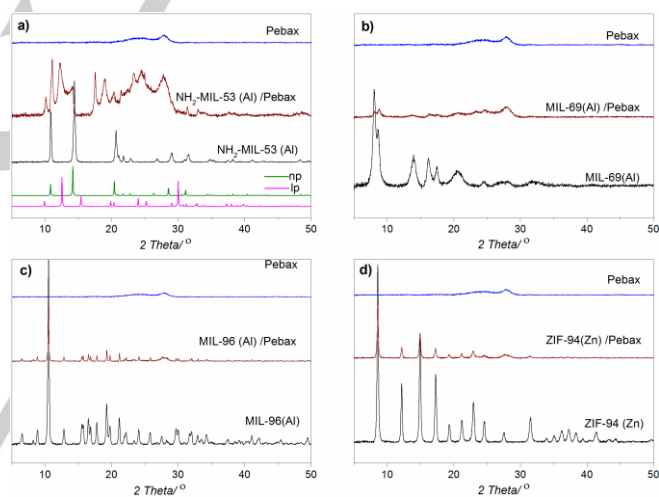


**Figure 7.** The XRD patterns of the MOF fillers, neat Pebax membranes and MMMs. The simulated XRD patterns of  $\text{NH}_2\text{-MIL-53(Al)}$  (*lp* and *np* forms) are shown for reference.

### MMM characterization

In order to benefit from the incorporation of MOF crystals in the polymeric matrix, membranes with a relatively high filler loading (25 wt. %) were prepared in this work. The SEM images in Figure 5 illustrate a good dispersion of the fillers independently of the MOF used. Differences in morphology can be appreciated when comparing 6FDA-DAM (Figure 5a, c, e and g), and Pebax membranes (Figure 5b, d, f and h), although this effect could be attributed to the more rigid

nature of 6FDA-DAM, the formation of such cavities during cryo-fracturing of these membranes cannot be discarded. As already anticipated above, XRD patterns of the pure MOFs (Figure. S1), demonstrate the absence of other phases and are in good agreement with the simulated diffraction patterns for each MOF. [47, 50, 52, 60] The as-synthesized sub-micrometre  $\text{NH}_2\text{-MIL-53(Al)}$  powders display the expected narrow pore configuration (Figure 6a and Figure 7a). [58] In MIL-69(Al) the narrow and large pore configuration seem to co-exist (Figure S1). 6FDA-DAM is fully amorphous with a broad diffraction peak between  $12\text{-}23^\circ$  (Figure 6), while Pebax shows a certain degree of crystallinity, as previously reported (Figure 7). [61] XRD patterns of the composites demonstrate that the crystalline structure of the MOFs was well retained upon MMM preparation. It should be noted that pore expansion of  $\text{NH}_2\text{-MIL-53(Al)}$  occurs in the presence of Pebax (Figure 7a), suggesting polymer penetration in the MOF porosity. [34]

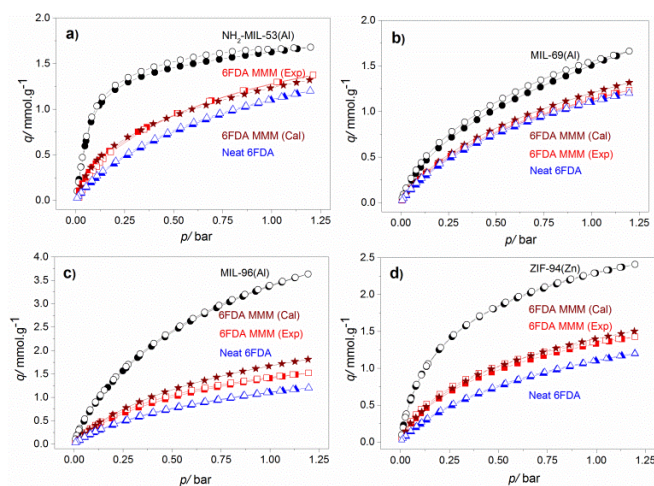


**Figure 8.** Experimental  $\text{CO}_2$  adsorption (solid symbols) and desorption (open symbols) isotherms of MOF fillers, neat 6FDA-DAM membrane and MMMs with filler loadings of 25 wt. % at 295 K. The calculated adsorption isotherms of MMMs are shown for comparison.

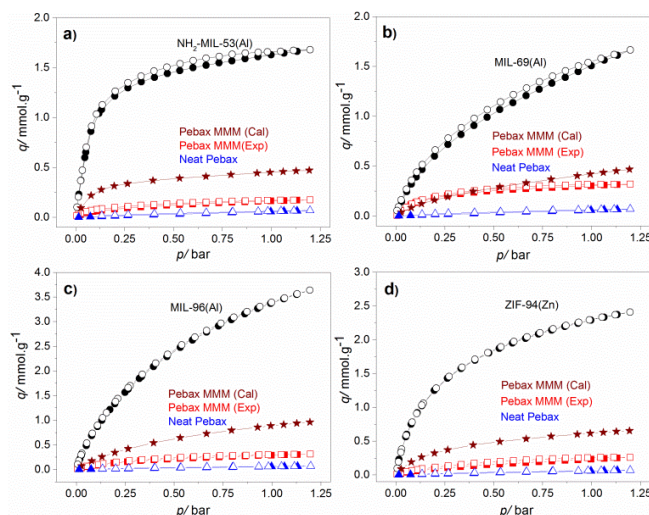


**Figure 9.** Experimental  $\text{CO}_2$  adsorption (solid symbols) and desorption (open symbols) isotherms of MOF fillers, neat Pebax membrane and MMMs with filler loadings of 25 wt. % at 295 K. The calculated adsorption isotherms of MMMs are shown for comparison.

Figure 8 shows the  $\text{CO}_2$  adsorption and desorption isotherms of MMMs with 6FDA-DAM as the continuous phase. All adsorption isotherms can be described as a linear combination (taking into account the ratio in the MMM) of the isotherms of their components (MOF and polymer), demonstrating that neither the MOF porosity nor the one related to the polymer are compromised upon membrane preparation.

The low free volume of Pebax is clearly exemplified in its corresponding  $\text{CO}_2$  adsorption (Figure 9). [61] In this case, the calculated adsorption isotherms for the MMMs based on Pebax do not correspond with the experimentally measured data, except for MIL-69(Al) MMM. A similar effect was earlier observed for MOF containing silicone rubber based MMMs [41] and can be attributed to the partial blocking of the MOF fillers by polymer penetration, except for MIL-69(Al) in view of its narrower window size. [47] The increased contribution of the larger pore size in the MMM may be due to a solvent effect.

### Gas permeation

The  $\text{CO}_2/\text{N}_2$  (15/85, mol/mol) mixed gas permeation results of the neat polymeric membranes and MMMs were evaluated at 2 bar absolute and 298 K, and compared with the pure gas  $\text{CO}_2$  permeation at 1 bar absolute displayed in Figure 10.

The  $\text{CO}_2$  permeabilities of the 6FDA-DAM membranes for the mixed gas are higher than for the pure gas feed experiments. The  $\text{CO}_2$  pressure in the latter is higher, approaching a more saturated membrane and a lower apparent permeability, while the molar permeation flow through the membrane is higher. In the case of Pebax, this difference between the mixed gas and pure gas

permeability is nearly absent, apart from MIL-69, so the diffusivity in the polymer phase will be the major controlling variable for these membranes. Although the relationship of Eq. (3) is therefore approximate, it helps interpreting the observations. The CO<sub>2</sub> solubility and diffusivity values are calculated in single gas (1.0 bar, Figure 10b and 10d) and mixed gas experiments (0.3 bar CO<sub>2</sub> partial pressure, Figure S2). Comparing these two cases, both the CO<sub>2</sub> solubility and diffusivity follow the same trend upon implanting various MOF fillers.

The CO<sub>2</sub> permeability of the bare 6FDA-DAM membranes was ca. 780 Barrer with a CO<sub>2</sub>/N<sub>2</sub> mixture selectivity of 24 (Figure 10a). After addition of NH<sub>2</sub>-MIL-53(Al), MIL-96(Al) and ZIF-94, the CO<sub>2</sub> permeability was enhanced (~35%, ~32% and ~42%, respectively) (Figure 10a) in virtue of the improved CO<sub>2</sub> solubility (Figure 10b and Figure S2a). The CO<sub>2</sub> diffusivity had hardly changed, with ZIF-94 as exception due to its 3D pore structure. The CO<sub>2</sub>/N<sub>2</sub> selectivity is slightly increased, the most for MIL-69(Al). Although this MOF possesses similar diamond-shaped 1D channels as NH<sub>2</sub>-MIL-53(Al), they are smaller in size,<sup>[47]</sup> explaining the higher selectivity, but lower permeability.

In comparison with neat 6FDA-DAM membranes, the bare Pebax membranes exhibit a higher CO<sub>2</sub>/N<sub>2</sub> selectivity (~57) and lower CO<sub>2</sub> permeability (~44 Barrer) (Figure 10c). Due to the increased CO<sub>2</sub> solubility (Figure 10d and Figure S2b), the CO<sub>2</sub> permeability of MIL-96(Al) and ZIF-94 based MMMs was improved (around 25% and 33%, respectively) together with a slight improvement in selectivity (Figure 10c). Interpreting the results in terms of Eq. (3) suggests that the CO<sub>2</sub> diffusivity dropped sharply upon incorporation of MOF fillers (Figure 10d and Figure S2b). This effect can be attributed to the partial blocking of the fillers or even penetration of the flexible Pebax chains (polyether segments) into the MOF pores. Also, the interaction between filler and polymer matrix may disturb the packing and rotation mobility of the polymeric chains, thus influencing its overall diffusion properties. No obvious performance enhancement in terms of CO<sub>2</sub> permeability was observed for the addition of MIL-69(Al) although its CO<sub>2</sub> solubility was boosted. This did result in an increase in selectivity attributed to the narrow pores of this MOF. Furthermore, the reduced CO<sub>2</sub> permeability of the NH<sub>2</sub>-MIL-53(Al)-Pebax membranes is a clear effect of polymer penetration.

In order to benchmark and to give a more general overview of membrane performance, the most relevant permeation data are plotted in Figure 11 along with the Robeson upper bound (CO<sub>2</sub>/N<sub>2</sub>, 2008).<sup>[9]</sup> Addition of the nonflexible, small pore 1D MOF MIL-69 results for both polymers in a slight increase in selectivity at almost constant permeability. In case of NH<sub>2</sub>-MIL-53, with a similar topology but a flexible structure, interaction with the polymer results either in a decrease in permeability (Pebax) attributed to polymer penetration into the MOF structure or in an

increase in permeability (6FDA-DAM) with hardly any improvement in selectivity, most likely related to a partial opening of the structure by the solvent upon membrane preparation.<sup>[60]</sup> Addition of the narrow pore, rigid, 2D-porous MIL-96 increases both permeability and selectivity for the two polymers. Finally, the 3D-porous ZIF-94 filler displays the largest increase in permeability for both polymers with a slight increase in selectivity only when Pebax is used as continuous phase. These results suggest that the MOF topology, dimensionality of porosity and interaction with the continuous polymer phase play key roles in determining membrane performance. The improved selectivity along with permeability (except for NH<sub>2</sub>-MIL-53(Al)-Pebax) moves the MMM performance closer to the upper bound limit.



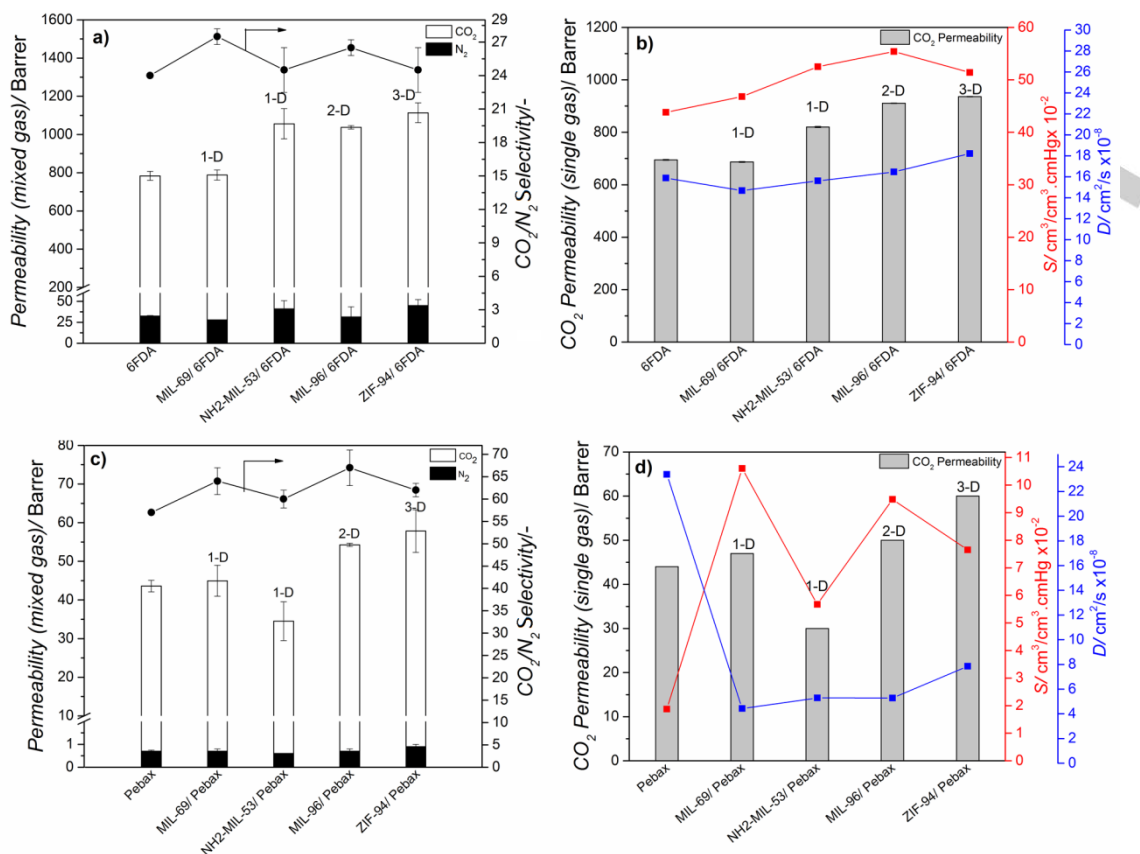


**Figure 10.** CO<sub>2</sub>/N<sub>2</sub> mixture permeability and selectivity of 6FDA-DAM (a) and Pebax (c) based membranes at 298 K and 2 bar absolute feed pressure (mixed gases). Single gas CO<sub>2</sub> permeability, solubility and diffusivity of 6FDA-DAM (b) and Pebax (d) based membranes at 295 K and 1 bar absolute feed pressure. Error bars correspond to standard deviation of duplicate membranes.

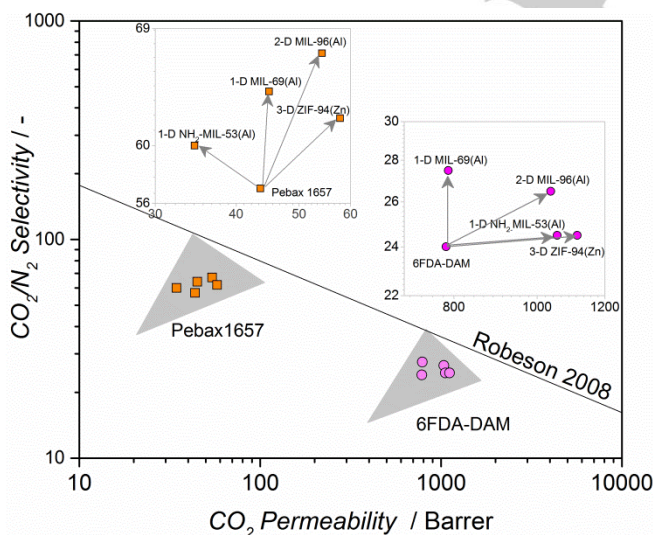


**Figure 11.** Robeson plot of CO<sub>2</sub> / N<sub>2</sub> couple (CO<sub>2</sub> selectivity versus permeability) of MOF-MMMs and neat 6FDA-DAM and Pebax membranes at 298 K and 2 bar absolute feed pressure (mixed gases). The insets are the enlarged views of the corresponding membrane performance. The Robeson upper bound (2008) is shown for reference. The MOF loading in all MMMs is 25 wt.%.

## Conclusions

Mixed matrix membranes (MMMs), composed of diverse MOF fillers (NH<sub>2</sub>-MIL-53(Al), MIL-69(Al), MIL-96(Al) and ZIF-94, 25 wt.% loading) and typical polymers (6FDA-DAM and Pebax) were developed for CO<sub>2</sub>/N<sub>2</sub> separation. The large adsorption capacity of MOF fillers at moderate pressure and possessing high porosity endows the 6FDA-DAM based MMMs with enhanced gas solubility. Consequently, an improved CO<sub>2</sub> permeability (~ 35%, 32% and 42% for NH<sub>2</sub>-MIL-53(Al), MIL-96(Al) and ZIF-94, respectively, relative to ~780 Barrer for neat 6FDA-DAM) was observed together with a slightly increased selectivity. In the case of Pebax based MMMs, the CO<sub>2</sub> permeability of MIL-96(Al) and ZIF-94 based Pebax-MMMs was boosted (~25% and 33%, respectively; ~44 Barrer for neat Pebax) along with a slight enhancement of selectivity because of the improved CO<sub>2</sub> solubility. The MMM performances are very close to the Robeson upper bound limit (2008, CO<sub>2</sub>/N<sub>2</sub>). The different pore structures of the MOF fillers, especially regarding their dimensionality, is responsible for the various performance modifications, although MOF-polymer interactions play another key role.



## Experimental Section

### Synthesis of MOF crystals

NH<sub>2</sub>-MIL-53(Al) submicrometer particles were synthesized according to a protocol reported earlier.<sup>[58]</sup> 1.5 g 2-amino-terephthalic acid (8.28 mmol, Sigma Aldrich, 99 %) and 1.97 g AlCl<sub>3</sub>·6H<sub>2</sub>O (8.43 mmol, Sigma Aldrich, ≥ 99.0 %) were dissolved in a solution containing 18 mL deionized water and 2 mL N,N-dimethylformamide (DMF, Sigma Aldrich, >99.9%). Afterwards, the solution was transferred to a Teflon-lined autoclave and heated at 423 K for 5 h in an oven under static conditions. After cooling, the resulting yellow powders were filtered under vacuum and washed with acetone. Subsequently, the powders were thoroughly activated in DMF at 423 K and methanol at 443 K for 15 h. Then, the powders were washed with acetone and dried at 393 K.

MIL-69(Al) submicrometer particles were synthesized under reflux for 5 h. 0.43 g 2,6-Naphthalenedicarboxylic acid (2 mmol, Alfa Aesar), 0.19 g NaOH (4.75 mmol, Acros organic, extra pur) and 1.50 g Al(NO<sub>3</sub>)<sub>3</sub>·9H<sub>2</sub>O (4 mmol, Carlo Erba, 99+%) were dissolved in a 10 mL DMF (Carlo Erba, pur) and 10 mL H<sub>2</sub>O. The reaction mixture was stirred under reflux for 5 h. The resulting product was filtered and washed with 30 mL DMF at 323 K under stirring for 5-6 h.

To synthesize MIL-96(Al), aluminium nitrate nonahydrate (4.5 g, 12 mmol) and trimesic acid (2.52 g, 12 mmol) were dissolved in 300 mL of a H<sub>2</sub>O/DMF (50/50, vol./vol.) mixture. Acetic acid (1.68 mL, 30 mmol) was added and the mixture was heated to reflux for 16 h. The resulting white mixture was centrifuged at 14500 rpm for 15 min, and then washed once with deionized water (100 mL), one more time with a H<sub>2</sub>O/EtOH (50/50, vol./vol.) mixture (100 mL) and finally with EtOH (100 mL). The white powder was dried at room temperature and pure MIL-96(Al) particles were obtained.

Synthesis of ZIF-94 involved dissolving 0.4392 g Zn(CH<sub>3</sub>COO)<sub>2</sub>·2H<sub>2</sub>O (2 mmol) in 20 mL methanol and 0.4404 g 4-methyl-5-imidazolecarboxaldehyde (mcim, 4 mmol) in 50 mL THF. After the solids were completely dissolved, Zn(CH<sub>3</sub>COO)<sub>2</sub>·2H<sub>2</sub>O-methanol solution was poured slowly into the mcim-THF solution. The mixture was continuously stirred for 60 min at room temperature. The product was collected by centrifugation and washed with methanol three times before drying at room temperature.

### Preparation of mixed-matrix membranes (MMMs)

Preparation of 6FDA-DAM based MMMs, is based on a previously reported method.<sup>[35]</sup> 6FDA-DAM (Mw ~272,000 Da, supplied by Akron) was degassed overnight at 453 K under vacuum. 0.40 g dried polymer was dissolved in 3.0 mL tetrahydrofuran (THF, Sigma Aldrich, ≥ 99.99 %). Then, 0.13 g of MOF crystals were suspended in 1.5 mL THF by ultrasonication and stirring. To attain better MOF and polymer interaction, firstly, a 10 % of the dissolved polymer was

added to the MOF solution and the suspension was further stirred for 2 h (priming). Subsequently, the remaining amount of polymer solution was added to the MOF suspension and stirred overnight. The solution was poured on a glass plate and casted by Doctor Blade with a gap of 80 μm. Then, the membrane was covered with a top-drilled box and dried overnight under THF-saturated atmosphere at ambient temperature. Finally, the dried membranes were peeled off and treated under vacuum at 433 K for 24 h.

For the preparation of Pebax based MMMs, 0.18 g Pebax 1657 (supplied by Arkema) was dissolved in 3.0 mL water/ethanol (30/70 wt./wt.) mixture at 80 °C under reflux (2h) to achieve a polymeric solution. Then, 0.06 g MOF was added to 1.5 mL water/ethanol (30/70 wt./wt.), ultrasonicated and stirred. A similar procedure as described above was used for the casting of the membranes. Finally, the membranes were dried overnight in a top-drilled box in solvent saturated atmosphere, and then, treated under vacuum at 353 K for 24 h.

The MOF content in the above MMMs ( $W_{MOF}/(W_{MOF}+W_{polymer})$ ) was 25 wt. % in all cases. As a reference, membranes based on the neat polymers were also prepared following an identical procedure. The thickness of all membranes is around 30-40 μm, according to the measurements performed with a digital micrometer (Mitutoyo) at different locations within each membrane and then averaged.

### Characterization

XRD patterns of MOF powders and the membranes were acquired in a Bruker-D8 Advance diffractometer using Co-K<sub>α</sub> radiation ( $\lambda = 1.78897\text{\AA}$ , 40 KV, 30 mA). The  $2\theta$  range (5-60°) was scanned using a step size of 0.02° and a scan speed of 0.2 s per step in a continuous scanning mode.

N<sub>2</sub> and CO<sub>2</sub> adsorption isotherms of MOFs and membranes were recorded in a Tristar II 3020 (Micromeritics) setup at 77 K and 295 K, respectively. Prior to the measurements, at least 100 mg of each sample (powder or membrane) were degassed at 423 K under vacuum for 16 h and subsequently used for adsorption measurements.

Scanning electron microscopy (SEM) experiments were performed in a Dual Beam Strata 235 (FEI) and AURIGA Compact (Zeiss) microscopes with a secondary electron detector operated at 5 kV. The membrane specimens were prepared by freeze-fracturing after immersion in liquid N<sub>2</sub> and coated with gold.

The TEM samples were prepared by applying a few drops of MOF dispersed in ethanol on a carbon-coated copper grid. TEM analysis was carried out in JEOL JEM-2010 microscope operated at 200 kV. An X-ray OXFORD detector, INCA energy TEM 100 model for microanalysis (EDS) and a bottom-mounted GATAN ORIUS SC600 imaging camera are equipped in the machine. Micrograph acquisition was performed with GATAN Digital Micrograph 1.80.70 software. By using TEM images, around 50 particles were selected and measured by Image J software to calculate the average particle size.

### Gas permeation experiments

The CO<sub>2</sub>/N<sub>2</sub> separation measurements were carried out in a home-made setup described elsewhere.<sup>[20]</sup> The membranes, with constant area (3.14 cm<sup>2</sup>), were cut from the casted films and mounted in a flange between two Viton® O-rings. A macroporous stainless steel disc (316L, 20 μm nominal pore size) was used as support. All the evaluated membranes were in their fresh stage without aging. The permeation module was placed inside an oven, where the temperature was set to 298 K. A flow mixture (133 ml·min<sup>-1</sup>, STP) of CO<sub>2</sub> (15 mol.%) and N<sub>2</sub> (85 mol.%) was applied as feed and helium (5 ml·min<sup>-1</sup>, STP) as a sweep gas. The feed pressure was adjusted to 2 bar absolute using a back-pressure controller at the retentate side while the permeate side was kept at atmospheric pressure (1 bar) for all measurements. The permeation results of the membranes were recorded after stabilization overnight to ensure steady state permeation. An online gas chromatograph (Interscience Compact GC) equipped with a packed Carboxen® 1010 PLOT (30 m x 0.32 mm) column and TCD detector was used to analyse the permeate stream. Single gas CO<sub>2</sub> permeation tests were conducted at 295 K and 1 bar absolute feed pressure.

Gas separation performance is defined by the selectivity ( $\alpha$ ) or separation factor, and the gas permeability ( $P$ ) of the individual components. The permeability for the component  $i$  ( $P_i$ ) was calculated as follows (Equation 1):

$$P_i = \frac{F_i \delta}{\Delta p_i A} \quad \text{Equation (1)}$$

where  $F_i$  denotes the molar flow rate of compound  $i$ ,  $\delta$  is the thickness of the membrane,  $\Delta p_i$  is the partial pressure difference of  $i$  across the membrane, and  $A$  is the membrane area. Although the SI unit for the permeability is mol·s<sup>-1</sup>·m·m<sup>-2</sup>·Pa<sup>-1</sup>, gas permeabilities are reported in Barrer, where 1 Barrer = 3.35 x 10<sup>-16</sup> mol·s<sup>-1</sup>·m·m<sup>-2</sup>·Pa<sup>-1</sup>.

The mixed gas selectivity ( $\alpha$ ) of CO<sub>2</sub> over N<sub>2</sub> was defined as the ratio of their permeabilities (Equation 2):

$$\alpha = \frac{P_{CO_2}}{P_{N_2}} \quad \text{Equation (2)}$$

The solubility ( $S_{CO_2}$ ) of CO<sub>2</sub> in the membranes (at 1 bar) was quantified from gas sorption measurements up to 1.2 bar at 295 K. The mmol/g unit at 1 bar was converted to cm<sup>3</sup>(STP)/cm<sup>3</sup>·cmHg by applying the densities of MOFs and polymers (Table. S2) to calculate solubility for the density of MMMs based on 25 wt. % of MOF loading. The diffusivity ( $D_{CO_2}$ ) (at 1 bar) of CO<sub>2</sub> is calculated from the permeability and solubility (Equation 3):

$$D_{CO_2} = \frac{P_{CO_2}}{S_{CO_2i}} \quad \text{Equation (3)}$$

## Acknowledgements

Financial support of the European Research Council under the European Union's Seventh Framework Programme (FP/2007-2013), M4CO2 project (608490) is gratefully acknowledged.

## Conflicts of interest

There are no conflicts of interest to declare.

**Keywords:** metal-organic framework • mixed matrix membrane • gas separation • polymer • pore structure

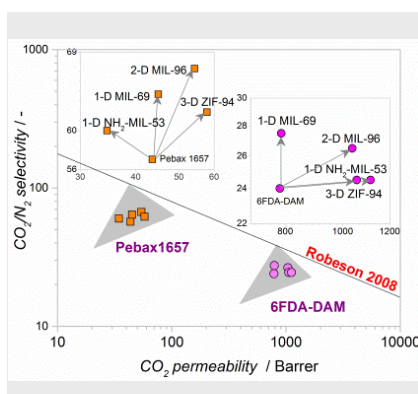
- [1] J. G. Vitillo, B. Smit, L. Gagliardi, *Chem. Rev.* **2017**, *117*, 9521–9523.
- [2] K. Sumida, D. L. Rogow, J. A. Mason, T. M. McDonald, E. D. Bloch, Z. R. Herm, T. H. Bae, J. R. Long, *Chem. Rev.* **2012**, *112*, 724–781.
- [3] A. Álvarez, A. Bansode, A. Urakawa, A. V. Bavykina, T. A. Wezendonk, M. Makkee, J. Gascon, F. Kapteijn, *Chem. Rev.* **2017**, *117*, 9804–9838.
- [4] B. Seoane, J. Coronas, I. Gascon, M. Etxeberria Benavides, O. Karvan, J. Caro, F. Kapteijn, J. Gascon, *Chem. Soc. Rev.* **2015**, *44*, 2421–2454.
- [5] W. J. Koros, R. P. Lively, *AIChE J.* **2012**, *58*, 2624–2633.
- [6] D. F. Sanders, Z. P. Smith, R. Guo, L. M. Robeson, J. E. McGrath, D. R. Paul, B. D. Freeman, *Polymer* **2013**, *54*, 4729–4761.
- [7] P. Bernardo, E. Drioli, G. Golemme, *Ind. Eng. Chem. Res.* **2009**, *48*, 4638–4663.
- [8] L. M. Robeson, *J. Membr. Sci.* **1991**, *62*, 165–185.
- [9] L. M. Robeson, *J. Membr. Sci.* **2008**, *320*, 390–400.
- [10] B. D. Freeman, *Macromolecules* **1999**, *32*, 375–380.
- [11] S. M. Saufi, A. F. Ismail, *Carbon* **2004**, *42*, 241–259.
- [12] J. Gascon, F. Kapteijn, B. Zornoza, V. Sebastián, C. Casado, J. Coronas, *Chem. Mater.* **2012**, *24*, 2829–2844.
- [13] N. Rangnekar, N. Mittal, B. Elyassi, J. Caro, M. Tsapatsis, *Chem. Soc. Rev.* **2015**, *44*, 7128–7154.
- [14] W. J. Koros, C. Zhang, *Nat. Mater.* **2017**, *16*, 289–297.
- [15] J. Dechnik, J. Gascon, C. J. Doonan, C. Janiak, C. J. Sumby, *Angew. Chem. Int. Ed.* **2017**, *56*, 9292–9310.
- [16] H. C. Zhou, J. R. Long, O. M. Yaghi, *Chem. Rev.* **2012**, *112*, 673–674.
- [17] S. Kitagawa, R. Kitaura, S. Noro, *Angew. Chem. Int. Ed.* **2004**, *43*, 2334–2375.
- [18] G. Férey, *Chem. Soc. Rev.* **2008**, *37*, 191–214.
- [19] A. J. Howarth, Y. Liu, P. Li, Z. Li, T. C. Wang, J. T. Hupp, O. K. Farha, *Nat. Rev. Mater.* **2016**, *1*, 15018.
- [20] T. Rodenas, I. Luz, G. Prieto, B. Seoane, H. Miro, A. Corma, F. Kapteijn, F. Llabre's i Xamena, J. Gascon, *Nat. Mater.* **2015**, *14*, 48–55.
- [21] X. L. Liu, Y. S. Li, G. Q. Zhu, Y. J. Ban, L. Y. Xu, W. S. Yang, *Angew. Chem. Int. Ed.* **2011**, *50*, 10636–10639.
- [22] T. H. Bae, J. S. Lee, W. Qiu, W. J. Koros, C. W. Jones, S. Nair, *Angew. Chem. Int. Ed.* **2010**, *49*, 9863–9866.
- [23] S. Sorribas, P. Gorgojo, C. Téllez, J. Coronas, A. G. Livingston, *J. Am. Chem. Soc.* **2013**, *135*, 15201–15208.
- [24] G. Dong, H. Li, V. Chen, *J. Mater. Chem. A* **2013**, *1*, 4610–4630.
- [25] S. Japip, K. S. Liao, T. S. Chung, *Adv. Mater.* **2017**, *29*, 1603833.
- [26] A. Knebel, S. Friebe, N. C. Bigall, M. Benzaqui, C. Serre, J. Caro, *ACS Appl. Mater. Interfaces* **2016**, *8*, 7536–7544.
- [27] L. Diestel, X. L. Liu, Y. S. Li, W. S. Yang, J. Caro, *Micropor. Mesopor. Mater.* **2014**, *189*, 210–215.
- [28] Y. Ban, Z. Li, Y. Li, Y. Peng, H. Jin, W. Jiao, A. Guo, P. Wang, Q. Yang, C. Zhong, W. Yang, *Angew. Chem. Int. Ed.* **2015**, *54*, 15483–15487.

- [29] Q. Song, S. Cao, R. H. Pritchard, H. Qiblawey, E. M. Terentjev, A. K. Cheetham, E. Sivaniah, *J. Mater. Chem. A* **2016**, *4*, 270-279.
- [30] Z. Wang, D. Wang, S. Zhang, L. Hu, J. Jin, *Adv. Mater.* **2016**, *28*, 3399-3405.
- [31] J. Sánchez-Lainez, B. Zornoza, S. Friebe, J. Caro, S. Cao, A. Sabetghadam, B. Seoane, J. Gascon, F. Kapteijn, C. L. Guillouzer, G. Clet, M. Daturi, C. Tellez, J. Coronas, *J. Membr. Sci.* **2016**, *515*, 45-53.
- [32] N. Tien-Binh, H. Vinh-Thang, X. Y. Chen, D. Rodrigue, S. Kaliaguine, *J. Mater. Chem. A* **2015**, *3*, 15202-15213.
- [33] B. Zornoza, A. Martinez-Joaristi, P. Serra-Crespo, C. Tellez, J. Coronas, J. Gascon, F. Kapteijn, *Chem. Commun.* **2011**, *47*, 9522-9524.
- [34] T. Rodenas, M. van Dalen, E. Garcia-Perez, P. Serra-Crespo, B. Zornoza, F. Kapteijn, J. Gascon, *Adv. Funct. Mater.* **2014**, *24*, 249-256.
- [35] A. Sabetghadam, B. Seoane, D. Keskin, N. Duim, T. Rodenas, S. Shahid, S. Sorribas, C. L. Guillouzer, G. Clet, C. Tellez, M. Daturi, J. Coronas, F. Kapteijn, J. Gascon, *Adv. Funct. Mater.* **2016**, *26*, 3154-3163.
- [36] J. Ma, Y. Ying, X. Guo, H. Huang, D. Liu, C. Zhong, *J. Mater. Chem. A* **2016**, *4*, 7281-7288.
- [37] N. C. Su, D. T. Sun, C. M. Beavers, D. K. Britt, W. L. Queen, J. J. Urban, *Energy Environ. Sci.* **2016**, *9*, 922-931.
- [38] S. R. Venna, M. Lartey, T. Li, A. Spore, S. Kumar, H. B. Nulwala, D. R. Luebke, N. L. Rosi, E. Albenze, *J. Mater. Chem. A* **2015**, *3*, 5014-5022.
- [39] S. J. D. Smith, C. H. Lau, J. I. Mardel, M. Kitchin, K. Konstas, B. P. Ladewig, M. R. Hill, *J. Mater. Chem. A* **2016**, *4*, 10627-10634.
- [40] J. Shen, G. Liu, K. Huang, Q. Li, K. Guan, Y. Li, W. Jin, *J. Membr. Sci.* **2016**, *513*, 155-165.
- [41] T. H. Bae, J. R. Long, *Energy Environ. Sci.* **2013**, *6*, 3565-3569.
- [42] S. Kanehashi, G. Q. Chen, L. Ciddor, A. Chaffee, S. E. Kentish, *J. Membr. Sci.* **2015**, *492*, 471-477.
- [43] J. Gascon, U. Aktay, M. D. Hernandez-Alonso, G. P. M. van Klink, F. Kapteijn, *J. Catal.* **2009**, *261*, 75-87.
- [44] C. Serre, F. Millange, C. Thouvenot, M. Noguès, G. Marsolier, D. Louër, G. Férey, *J. Am. Chem. Soc.* **2002**, *124*, 13519-13526.
- [45] S. Couck, J. F. M. Denayer, G. V. Baron, T. Rémy, J. Gascon, F. Kapteijn, *J. Am. Chem. Soc.* **2009**, *131*, 6326-6327.
- [46] E. Stavitski, E. A. Pidko, S. Couck, T. Remy, E. J. M. Hensen, B. M. Weckhuysen, J. Denayer, J. Gascon, F. Kapteijn, *Langmuir*, **2011**, *27*, 3970-3976.
- [47] T. Loiseau, C. Mellot-Draznieks, H. Muguerra, G. Férey, M. Haouas, F. Taulelle, *C. R. Chimie* **2005**, *8*, 765-772.
- [48] I. Senkovska, F. Hoffmann, M. Fröba, J. Getzschmann, W. Böhlmann, S. Kaskel, *Micropor. Mesopor. Mater.* **2009**, *122*, 93-98.
- [49] M. Benzaqui, R. S. Pillai, A. Sabetghadam, V. Benoit, P. Normand, J. Marrot, N. Menguy, D. Montero, W. Shepard, A. Tissot, C. Martineau-Corcoc, C. Sicard, M. Mihaylov, F. Carn, I. Beurroies, P. L. Llewellyn, G. De Weireld, K. Hadjiivanov, J. Gascon, F. Kapteijn, G. Maurin, N. Steunou, C. Serre, *Chem. Mater.* **2017**, *29*, 10326-10338.
- [50] T. Loiseau, L. Lecroq, C. Volkringer, J. Marrot, G. Férey, M. Haouas, F. Taulelle, S. Bourrelly, P. L. Llewellyn, M. Latroche, *J. Am. Chem. Soc.* **2006**, *128*, 10223-10230.
- [51] M. Maes, L. Alaerts, F. Vermoortele, R. Ameloot, S. Couck, V. Finsy, J. F. M. Denayer, D. E. De Vos, *J. Am. Chem. Soc.* **2010**, *132*, 2284-2292.
- [52] W. Morris, N. He, K. G. Ray, P. Klonowski, H. Furukawa, I. N. Daniels, Y. A. Houndonougbo, M. Asta, O. M. Yaghi, B. B. Laird, *J. Phys. Chem. C* **2012**, *116*, 24084-24090.
- [53] S. Aguado, J. Canivet, D. Farrusseng, *Chem. Commun.* **2010**, *46*, 7999-8001.
- [54] X. Liu, Y. Li, Y. Ban, Y. Peng, H. Jin, W. Yang, K. Li, *Mater. Lett.* **2014**, *136*, 341-344.
- [55] K. S. Park, Z. Ni, A. P. Côté, J. Y. Choi, R. Huang, F. J. Uribe-Romo, H. K. Chae, M. O'Keeffe, O. M. Yaghi, *Proc. Natl. Acad. Sci. U. S. A.* **2006**, *103*, 10186-10191.
- [56] S. Aguado, C.-H. Nicolas, V. Moizan-Basle, C. Nieto, H. Amrouche, N. Bats, N. Audebrandt, D. Farrusseng, *New J. Chem.* **2011**, *35*, 41-44.
- [57] F. Cacho-Bailo, M. Etxeberria-Benavides, O. Karvan, C. Tellez, J. Coronas, *CrystEngComm* **2017**, *19*, 1545-1554.
- [58] T. Rodenas, M. van Dalen, P. Serra-Crespo, F. Kapteijn, J. Gascon, *Micropor. Mesopor. Mater.* **2014**, *192*, 35-42.
- [59] S. Couck, E. Gobechiya, C. E. A. Kirschhock, P. Serra-Crespo, J. Juan-Alcañiz, A. Martinez Joaristi, E. Stavitski, J. Gascon, F. Kapteijn, G. V. Baron, J. F. M. Denayer, *ChemSusChem* **2012**, *5*, 740-750.
- [60] P. Serra-Crespo, M. A. van der Veen, E. Gobechiya, K. Houthoofd, Y. Filinchuk, C. E. A. Kirschhock, J. A. Martens, B. F. Sels, D. E. De Vos, F. Kapteijn, J. Gascon, *J. Am. Chem. Soc.* **2012**, *134*, 8314-8317.
- [61] J. H. Kim, S. Y. Ha, Y. M. Lee, *J. Membr. Sci.* **2001**, *190*, 179-193.



## FULL PAPER

**1D, 2D, 3D pores:** Influence of MOF fillers with various chemical functionalities, topologies, and dimensionalities of porosity and polymers on the performance of mixed matrix membranes were studied. The changes in performance were rationalized on the basis of gas solubility, diffusivity and phase compatibility.



A. Sabetghadam, X. Liu,\* M. Benzaqui, E. Gkaniatsou, A. Orsi, M. M. Lozinska, C. Sicard, T. Johnson, N. Steunou, P. A. Wright, C. Serre, J. Gascon, F. Kapteijn\*

Page No. – Page No.

**Influence of Filler Pore Structure and Polymer on the Performance of MOF-based Mixed Matrix Membranes for CO<sub>2</sub> Capture**